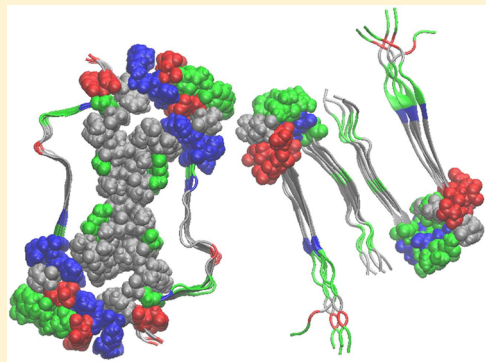


Stability of Osaka Mutant and Wild-Type Fibril Models

Workalemahu M. Berhanu, Erik J. Alred, and Ulrich H. E. Hansmann*

Department of Chemistry & Biochemistry, University of Oklahoma, Norman, Oklahoma 73019, United States

ABSTRACT: Single amino acid mutations in amyloid-beta ($A\beta$) peptides can lead to early onset and increased severity of Alzheimer's disease. An example is the Osaka mutation ($A\beta_{1-40}E22D$), which is more toxic than wild-type $A\beta_{1-40}$. This mutant quickly forms early stage fibrils, one of the hallmarks of the disease, and these fibrils can even seed fibrilization of wild-type monomers. Using molecular dynamic simulations, we show that because of formation of various intra- and intermolecular salt bridges the Osaka mutant fibrils are more stable than wild-type fibrils. The mutant fibril also has a wider water channel with increased water flow than the wild type. These two observations can explain the higher toxicity and aggregation rate of the Osaka mutant over the wild type.



INTRODUCTION

Protein aggregation is a factor common to various neurodegeneration diseases, including Alzheimer's disease.¹ The latter is characterized by neuronal deposits of $A\beta$ fibrils.^{2,3} Although oligomeric aggregates seem to be the main cause for the loss of neuronal function,⁴ the thermodynamically more stable amyloid fibrils are also toxic to cell cultures.^{5,6} Likely, both $A\beta$ fibrils and oligomers cause neurodegeneration, and therefore both should be considered when therapeutic agents are developed.⁵ Amyloids form by the self-association of misfolded proteins into transient oligomers of various sizes. Once a nucleation threshold is reached, oligomers with appropriate structures become stable and act as seeds for the growth of fibrils.⁵ The end state is an equilibrium between oligomers and fibrils where dissociation and association occur continuously.⁵ *In vitro*, both oligomers and amyloid fibrils are characterized by polymorphism. For instance, at least five different structures of $A\beta_{40}$ amyloid fibrils have been determined by ssNMR, and it is expected that more will be found in the future.⁵ The differences in molecular structure between these amyloid fibril polymorphs correlate with speed of disease progress,^{7,8} and it is conjectured that these "strains" can propagate prion-like in Alzheimer patients,^{9,10} which may explain why no polymorphism is found in fibril taken from patient brains.

Various mutations can lead to rare familial variants of Alzheimer's disease that are characterized by early onset and/or more severe symptoms. The differences in pathogenesis are related to the higher neurotoxicity and an increase in aggregation propensity of the amyloid fibrils formed by these mutants. Hence, comparing the fibril structures of such mutants with the wild-type $A\beta$ aggregates allows one to probe the relation between fibril structure and disease progression. One example is the Osaka mutant ($\Delta E_{22}-A\beta_{1-39}$), which lacks the glutamate found in the wild type¹¹ at position 22 and rapidly forms fibrils in solution.¹² The fibril formed *in vitro* by the

Osaka mutant has a 2-fold symmetry but differs strongly in its quaternary structure from previously proposed fibril models of wild-type $A\beta_{1-40}$.⁷ Instead of the simple U-shaped (hairpin) model of the wild-type $A\beta_{1-40}$, the Osaka structure consists of parallel in-register strands whose arrangement resembles a cinnamon roll (Figure 1). It has been suggested that this fold could also be found for other familial mutants where the E22 residue is not deleted but replaced by another residue located very close to E22⁷ of $A\beta$ wild-type sequence.⁷

Though the wild-type $A\beta_{1-40}$ fibril structures have been extensively studied,¹³ less is known about the energetics and the mechanism of aggregation of the Osaka mutant or related familial mutants.⁷ The missing detailed molecular level characterization of their structures and building principles may allow us to pinpoint the cause for the higher aggregation propensity of the Osaka mutant and the reason why preformed $A\beta_{1-40} E_{22}\Delta$ fibrils are very efficient in cross-seeding $A\beta$ wild-type aggregates, but not the other way around. Such characterization may also explain the higher toxicity of Osaka mutant. One way to probe the atomic-level structural dynamics and the thermodynamics of such β -sheet oligomers^{14,15} is by molecular dynamics simulations. Such simulations have been used in the past extensively to explore the structure of such oligomers and the pathways of their oligomerization,^{16,14} and they have been shown to be valuable tools for characterizing the structural transitions involved in $A\beta$ fibril elongation.^{17,18} In this paper, we utilize molecular dynamics simulations to obtain a deeper insight into aggregation propensity of the wild type and Osaka mutant and into the growth of $A\beta$ wild-type monomer on preformed $A\beta_{1-40} E_{22}\Delta$ nuclei. In this way, we hope to derive rules that may be useful for predicting structure of other familial mutants especially those where the mutation is

Received: August 17, 2015

Revised: September 23, 2015

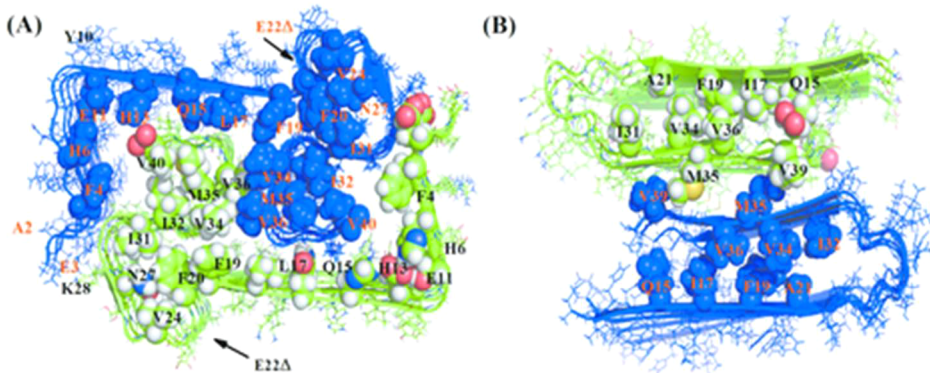


Figure 1. Comparison of the *in vitro* 2-fold symmetry ssNMR structural models of the Osaka mutant (pdb id: 2mvx) and the recent wild-type A β _{1–40} fibril models of Bertini. (A) The Osaka mutant model has a rectangular shape that resembles a cinnamon roll. The central part is characterized by strong hydrophobic interactions that contribute to the stability of the structure. The intermolecular salt bridge between E3 and K28 plays a significant role in maintaining its highly ordered structure. (B) The wild-type model consists of two U-shaped units with strand-loop-stand contacts L17/V36, F19/L34, A21/I32, and an intersheet contact V39/M35. The amino acid side chain contacts (interstrand and intersheet) in both models are displaced as spheres. We have colored in blue and green the two strand-loop-stand units of the double layer.

close the E22 (such as A β _{1–40}E₂₂G [Arctic] and A β _{1–40}E₂₂Q [Dutch]).

Given current computational constraints it is not possible to simulate at atomic detail directly the spontaneous fibril formation of full length wild-type A β and the Osaka mutant, or of the growth of wild-type A β peptides on Osaka mutant¹⁷ nuclei. However, information on these processes can be obtained in an indirect way by contrasting the stability of Osaka mutant and A β wild type, a computationally more feasible task. Hence, multiple long trajectories starting from preformed wild type and Osaka mutant¹⁷ fibril-like oligomer are obtained by molecular dynamics simulations at constant temperature simulation to evaluate the stability of wild-type and mutant aggregates. These simulations will address the following questions: (1) What is the role of the large number of salt bridges for the structural stability of the Osaka mutant fibril? (2) How does the difference in the pore size affect hydration dynamics and how is it related to aggregation growth and toxicity? (3) How does the fibril organization (quaternary structure) in the two systems leads to the observed differences in seeding propensities?

MATERIALS AND METHOD

Fibril Model Construction. The existing A β wild-type fibril structures as obtained by ssNMR can be classified into two forms: with a 2-fold symmetry of their quaternary structure and with a 3-fold symmetry. We have shown in recent all-atom explicit-solvent molecular dynamics simulations that 2-fold structures are more stable.¹⁹ For this reason, we use here for our wild-type A β simulations the structure recently reported by Bertini et al.,²⁰ which differs slightly from earlier A β _{1–40} fibril polymorphs with 2-fold symmetry in the contacts among amino acid side chains within the strand-loop-strand hairpins, and between these units and an additional β strand segment in the N-terminal tail. We choose this model because it is the most recent solid-state NMR derived experimental fibril model, and because the presence of an additional N-terminal methionine in well-organized fibril samples of A β 40 has led to high-resolution spectra resulting in a very accurate structural model. Using this model (the coordinates were kindly provided by Dr. Claudio Luchinat), we build ten-layer systems by aligning two five-layer systems, made each of two strand-loop-strand hairpins,

such that intersheet distances are 7.4 Å and there is a negative staggering between the two β -sheet layers. For the Osaka mutant we did not need to construct a model. Instead we used the double-layer ten-strand structure (pdb id: 2mvx) by Schutz et al.⁷ that consists of 10 strands with two β -sheets that have parallel in-register strands forming a ‘‘cinnamon roll’’. Note that the Osaka mutant structure used in our simulation lacks the staggering⁷ that has been observed in the ssNMR structure of the wild-type A β .²¹ Also note that for generating these models we use the first model of the respective NMR ensembles. Both the Osaka mutant model and the wild-type model are shown in Figure 1.

Simulation Protocol. The stability of the Osaka mutant and A β wild-type decamers was probed using three independent all-atom molecular dynamic simulations with an AMBER ff99SB force field²² for the protein and a (TIP3P)²³ model for the explicit solvent, using the GROMACS program version 4.6.5-dp.²⁴ A cubic box, centered on the protein, was generated with a distance from the edge of the box to the protein of at least 12 Å. Because of the use of periodic boundary condition we use a PME algorithm for calculation of electrostatic interactions.²³ A 2 fs time step was selected, and the LINCS²⁵ algorithm is used to constraint hydrogens, whereas the Settle algorithm²⁶ was used for the solvent. The simulations were run at a constant temperature of 310 K, maintained by the Parrinello–Donadio–Bussi algorithm²⁷ ($\tau = 0.1$ fs),^{27,28} and the pressure of 1 bar was set with the Parrinello–Rahman algorithm²⁹ ($\tau = 1$ fs).

The solvated protein is first relaxed to an energy-minimized state; then it is equilibrated first using a NVT ensemble for 2 ns and second using a pressure coupled NPT ensemble for another 2 ns run. Subsequently, molecular dynamics simulations of 100 ns are run in an NPT ensemble for both Osaka mutant and wild-type A β decamers. Three separate trajectories starting from different initial velocities were generated for each system. Due to the use of the same initial structure, these trajectories are not wholly independent, which means error estimates may not be entirely realistic. Data were saved every 4 ps to allow for analysis with the tools available in GROMACS. The following values were measured to discern structural evolution: root-means-square deviations of the C α atoms (RMSD), water content within the oligomer cavity, water flow rates within the

oligomer cavity, pore diameter of the oligomer cavity, secondary structure contents, salt bridge distances (in the Osaka mutant) and hydrogen bonds. Imaging and visualization were performed using PYMOL. VMD scripts are used for analysis of the water content and flow rates.³⁰ The binding energy (in units of kcal/mol) between the two half-units of the decameric fibrils is evaluated using the MM/GBSA method implemented in AMBER 14 package.³¹

RESULTS AND DISCUSSION

Structural Stability of Osaka Mutant and Wild-Type

A β Oligomers. One way to evaluate the stability of aggregates is by comparing the final and initial structures of a sufficiently long molecular dynamics simulation run at a physiologically relevant temperature. Visual inspection of the structures obtained after 100 ns at 310 K shows for all three trajectories little change from the initial fibril structure of the Osaka mutant oligomer (Figure 2). On the contrary, the A β wild-type

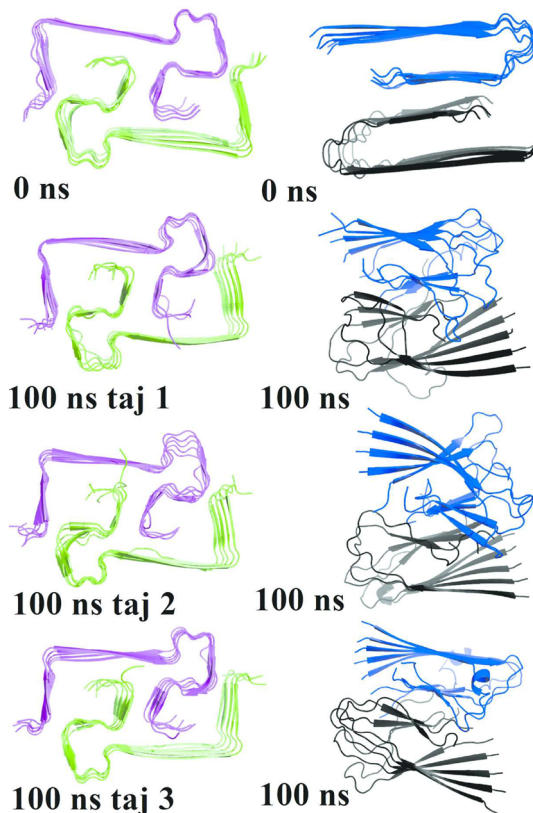


Figure 2. Snapshots of the Osaka mutant and A β wild-type fibril models at the start and end of a 100 ns molecular dynamics simulation. The 2-fold units of the Osaka mutant are magenta and green for clarification. The wild-type 2-fold units are in black and blue.

oligomer changes along the trajectories, with the differences between final and initial structure especially pronounced in the highly flexible region of the outer chains and the turn region of the U-shaped β -sheets (Figure 2). However, despite the larger flexibility, we see no separation of monomer from the oligomers for the A β wild type. These observations are quantified by the C α -RMSD (root-mean-square deviation) values between the final and initial configurations listed in (Table 1). For the rectangular-shaped two layer β -sheets of Osaka mutant decamers we find an average value of \sim 3.3 Å root-mean-

Table 1. Average C α RMSD (Å), Channel Diameter (Å), Main Chain Hydrogen Bonds, and Average Number of Water Molecules Inside the Channel of the Osaka Mutant and Wild Type

type of analysis	run	Osaka mutant	A β wild type
C α RMSD (Å)	1	3.4	5.4
	2	3.4	5.2
	3	3.2	5.4
mean value \pm SD ^a		3.3 \pm 0.1	5.3 \pm 0.1
main chain hydrogen bonds	1	201.8	123.8
	2	196.2	122.4
	3	203.4	119.8
mean value \pm SD		200.5 \pm 3.8	122.0 \pm 2.0
pore diameter (Å) of the first channel (1 β -sheet)	1	18.1	11.5
	2	18.4	7.6
	3	18.1	10.7
mean value \pm SD		18.2 \pm 0.2	9.9 \pm 2.1
pore diameter (Å) of the second channel (2 β -sheet)	1	21.1	11.2
	2	20.8	12.1
	3	20.4	10.1
mean value \pm SD		20.8 \pm 0.4	11.1 \pm 1.0
av no. of water molecules in fibrils interior	1	63	17
	2	60	23
	3	60	24
mean value \pm SD		61.0 \pm 1.7	21.3 \pm 3.8
water flow (ns ⁻¹)	1	29.4	10.5
	2	31.2	14.3
	3	29.2	12.1
mean value \pm SD		30.0 \pm 1.1	12.3 \pm 1.9

^aMean values and standard deviation (SD) are calculated from the three values obtained by averaging over the last 25 ns of each of the three independent runs of each model.

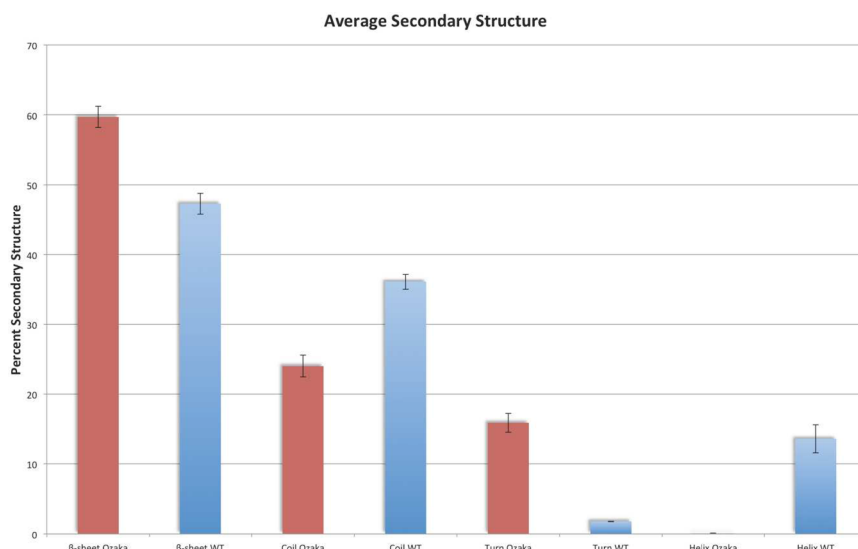
square-deviation whereas the corresponding value for A β wild-type oligomers is in the range of 5.2–5.4 Å (Table 1).

To quantify the differences in stability between Osaka mutant and wild-type A β , we compare the binding free energy of the Osaka mutant and that of the wild-type A β . This quantity describes how favorable it is to combine two smaller oligomers (of half the size) to a decamer.³² We approximate this binding energy by the MM-GBSA method as implemented in AMBER 14, using for the calculations the last 20 ns of our trajectories during which we extract 2500 snapshots separated by a time interval of 8 ps.

In terms of both accuracy and computational costs, the MM/GBSA method is halfway between empirical scoring (low cost and low accuracy) and rigorous alchemical perturbation methods (very accurate but costly). The main drawback of MM/GBSA is that the entropy term calculation is questionable due to the lack of the conformational contribution from binding-site water molecules as there is no information about how many water molecules there are in the binding site and their entropy before and after the ligand binding. There is also a problem of poor convergence of the simulated entropies.^{33,34} Despite its limitations resulting from severe approximations,³⁴ the method can be often used to reproduce and rationalize experimental findings. This is because the vibrational entropy contributes only a small fraction to the total energy³⁵ in computer simulations that model polymorphism of amyloid

Table 2. MM-PBSA-Calculated Free Energy with Its Components (kcal/mol) for Osaka Mutant and Wild Type upon Combining Two Halves of the Aggregate

system	ΔE_{vdW}	ΔE_{ele}	ΔG_{GB}	ΔG_{Sur}	ΔG_{Bind}
Osaka Fibril					
Traj1	-312.0	-426.6	572.4	-40.6	-206.8
Traj2	-266.7	-684.8	793.8	-38.2	-195.9
Traj3	-270.2	-386.9	515.5	-37.3	-178.9
mean value \pm SD	-283.0 \pm 25.2	-449.0 \pm 161.7	627.2 \pm 147.0	-38.7 \pm 1.7	-193.9 \pm 14.1
$\text{A}\beta$ Wt fibril					
Traj1	-166.8	-7.5	90.8	-21.4	-104.8
Traj2	-162.9	-4.7	96.4	-16.9	-87.40
Traj3	-154.9	-7.5	90.8	-21.4	-104.8
mean value \pm SD	-161.5 \pm 6.1	-6.6 \pm 1.6	93.6 \pm 3.9	-19.9 \pm 2.6	-99.0 \pm 10.0

**Figure 3.** Percentage of secondary structure of the Ozaka (red) and wild type (blue) for the last 25 ns of the simulation as predicted by DSSP and averaged between the three trajectories.

aggregates or the effect of single point mutants on fibril stability.

The results of our MM/GBSA calculations in Amber 14 are shown in Table 2. The binding energies ΔG (Table 2) for the Osaka mutant indicate it is more structurally favorable by about 100 kcal/mol (\sim 200 kcal/mol) than the wild type. The energetics of both fibril oligomers is dominated by the apolar terms (ΔE_{vdW} and ΔG_{sur}), especially by the vdW term. The interpentameric (between the two halves of the fibril oligomers) van der Waals term and the nonpolar solvation terms (ΔG_{sur}) are the most significant contributions of energy for the stabilization of the fibril oligomer. Binding is disfavored by the electrostatic term in the solvation free energy ΔG_{GB} , whereas ΔE_{ele} , the electrostatic interaction between sheets, favors binding. However, in each case, the less favorable electrostatic term is offset by the nonpolar component of the free energy, especially the van der Waals energy E_{vdW} as opposed to the nonpolar component of solvation term (ΔG_{sur}); and the contribution of these two terms is higher in the Osaka mutant (Table 2). Hence, the larger hydrophobic interaction in the quaternary structure of the mutant seems to account for a faster aggregation in the mutant than is seen for the wild type. Note that the entropy term in our MM/GBSA calculation has not been calculated, as its contribution to the total energy is expected to be small, and because it can only be crudely estimated. For this reason, the entropy term is, as in our case,

usually neglected in the determination of the relative binding free energies of very similar-sized molecules.³⁶

In summary, visual inspection and free energy analysis of our simulations suggest that the Osaka mutant forms more stable nucleation units than the wild type. We note that a number of previous simulations^{37,38} using a variety of force fields found slightly better stability for the double-layer wild-type $\text{A}\beta$ reported by Tycko in 2006³⁹ than we find for the Bertini wild-type model. This small difference in structural stability is likely due to the slightly different intersheet and intrastrand contacts in both models; however, it does not change the overall picture that the Osaka mutant forms more stable nucleation units than the wild type. The existence of already very stable small nuclei may explain the instantaneous fibril formation that is found for the Osaka mutant in *in vitro* experiments.

Secondary Structure, Backbone Hydrogen Bonding, and a Dynamic Network of Salt Bridge Stabilizes the Mutant More Than the Wild Type. The β -sheet content and the stability of amyloids are strongly correlated^{40,19} as the stability of amyloid fibrils is to a large extent determined by the interbackbone (main chain) hydrogen bonding network that connects individual β -strands⁴¹ in the cross- β structural motif common to amyloid fibrils. Such intermolecular hydrogen bonding contributes about 20 times more to structural rigidity than side-chain interactions between β -sheets.⁴¹ Hence, one can

expect that an amyloid form is the more stable, the more hydrogen bonds and the higher the β -sheet content. The larger average number of backbone hydrogen bonds (~ 200) in the more stable Osaka mutant decamer as compared to the number for the less stable wild-type aggregates (~ 122) in Table 1 is consistent with this assumption.

Using the DSSP⁴² software, we have also compared over the last 25 ns of our trajectories the secondary structure of the wild types and the Osaka mutant oligomers. The Osaka mutant fibril oligomers have an average β -sheet content of $60 \pm 2\%$, whereas the corresponding value for the wild-type $A\beta$ oligomers is one of $47 \pm 1\%$ (Figure 3). These numbers suggest that the interaction between neighboring β -strands that have higher β -sheet content leads for the Osaka mutant peptides to a more favorable binding than seen between the wild-type chains, which have a smaller β -sheet content per strand.³²

The Osaka mutant fibril structure⁷ is characterized by a salt bridge network in the fibril core consisting of ionic intraresidue interactions between H6 with E11, E11 with H13, H13 with Glu11, and H13 with the V39 terminal carboxyl group (Figure 4). The Osaka mutant also forms an *intermolecular* salt bridge

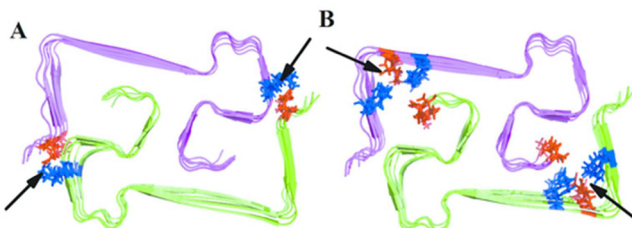


Figure 4. Salt bridge network of the Osaka mutant fibril oligomer. (A) The structure shows the intermolecular salt bridge between E3 and K28 of Osaka mutants. (B) The Osaka mutant structure has an intramolecular salt bridge consisting of three ionic intraresidue interactions between H6 with E11, E11 with H13, H13 with E11, and H13 with V39. Charged residues are red when they are negatively charged and blue when they are positively charged.

between E3 and K28, in which the extreme edge of N-terminal residues are attached to the fibril core leading to a highly ordered structure. This salt bridge may be the reason for the Osaka mutant being more stable than the wild type⁷ where residue K28 is part of an *intramolecular* salt bridge,⁸ and therefore the N-terminus is not as tightly attached to the fibril core as for the Osaka mutant.^{19,20,43} The stabilization of the N-terminus via an *intermolecular* salt bridge to K28 has been suggested as the key structural motif in mutants that cause early onset Alzheimer disease.⁴³ Note that *intramolecular* salt bridges⁸ between oppositely charged D23 and K28 side chains have been found by ssNMR in wild-type $A\beta$ 40 fibril polymorphs,^{8,39} but not in all polymorphs.^{39,20} For instance, the structure used in our simulation does not have this salt bridge. The lack of N terminal stabilization in the wild type may decrease its chance to act as nucleation seed, which in turn may explain why the wild type has a lower propensity for aggregation than the Osaka mutant with its N-terminal stabilization.^{43,44}

Hence, to investigate the role of such salt bridges, we have analyzed the *intermolecular* salt bridge between E3 and K28 of adjacent β -sheets of the Osaka mutant. This *intermolecular* salt bridge can occur in the Osaka mutant between ${}_1E_n^3$ and ${}_2K_n^{28}$ (and ${}_2E_n^3$ and ${}_1K_n^{28}$) or between ${}_1E_n^3$ and ${}_2K_{n-1}^{28}$ (and ${}_2E_n^3$ and

${}_1K_{n-1}^{28}$), where n marks for the peptide chain number, 1 stands for the first β -sheet, 2 stands for the second β -sheet. For locating salt bridges we measure the distance between the O atom of the C=O bonds of the carboxyl group in E3 to the N atom of the NH_3^+ group in K28. We define a *direct* salt bridges by the condition that this distance is around 4.3 Å, whereas an *indirect* or *water-mediated* salt bridge is assumed to have a distance within the range 4.3–7.0 Å.⁴⁵ We show in Figures 5

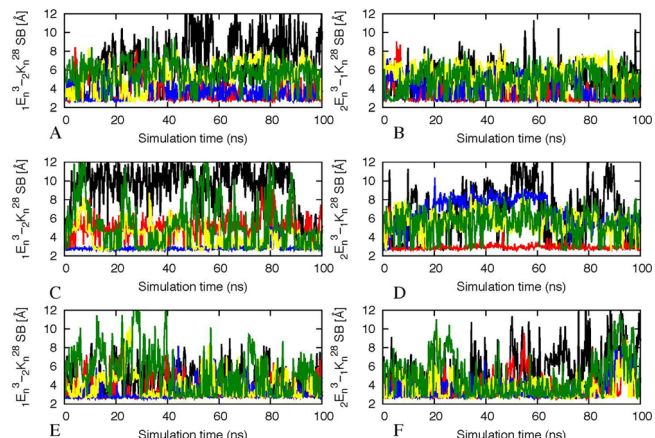


Figure 5. Average salt bridge interactions distances between ${}_1E_n^3$ and ${}_2K_n^{28}$ and ${}_1K_n^{28}$ for the Osaka mutant. The results shown are along the 100 ns of each trajectory. Key: (A) ${}_1E_n^3$ and ${}_2K_n^{28}$ for the first run; (B) ${}_2E_n^3$ and ${}_1K_n^{28}$ for the first run; (C) ${}_1E_n^3$ and ${}_2K_n^{28}$ for the second run; (D) ${}_2E_n^3$ and ${}_1K_n^{28}$ for the second run; (E) ${}_1E_n^3$ and ${}_2K_n^{28}$ for the third run; (F) ${}_2E_n^3$ and ${}_1K_n^{28}$ for the third run. Color: black, ${}_1E_n^3-2K_1^{28}$; red, ${}_1E_n^3-2K_2^{28}$; blue, ${}_1E_n^3-2K_3^{28}$; green, ${}_1E_n^3-2K_4^{28}$; yellow, ${}_1E_n^3-2K_5^{28}$.

and 6 that the extended ladders of salt bridges along the interface of the N terminal E3 and the K28 of the fibril core is dynamic. For most of the trajectories, the distances are within the range 4.3–7.0 Å; hence, this salt bridge is mediated through water molecules as the E3 is on the extreme end of the N-

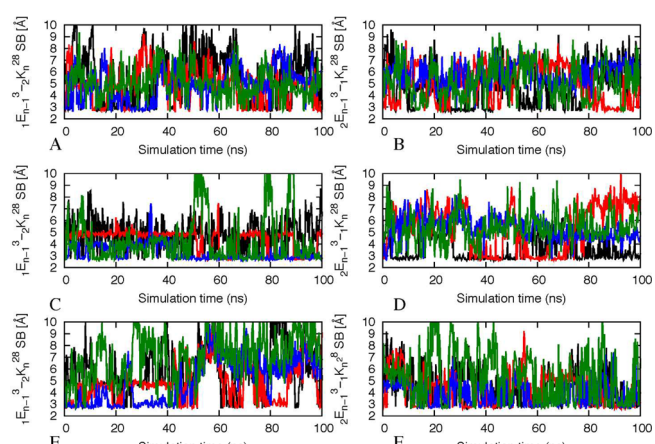


Figure 6. Average salt bridge distances between ${}_1Glu_n^3$ and ${}_2Lys_n^{28}$ and ${}_1K_n^{28}$ of the Osaka mutant. The results are shown along the 100 ns of each trajectory. Key: (A) ${}_1E_n^3$ and ${}_2K_{n-1}^{28}$ for the first run; (B) ${}_2E_n^3$ and ${}_1K_{n-1}^{28}$ for the first run; (C) ${}_1E_n^3$ and ${}_2K_{n-1}^{28}$ for the second run; (D) ${}_2E_n^3$ and ${}_1K_{n-1}^{28}$ for the second run; (E) ${}_1E_n^3$ and ${}_2K_{n-1}^{28}$ for the third run; (F) ${}_2E_n^3$ and ${}_1K_{n-1}^{28}$ for the third run. Color: black, ${}_1E_2^3-2K_1^{28}$; red, ${}_1E_3^3-2K_2^{28}$; blue, ${}_1E_4^3-2K_3^{28}$; yellow, ${}_1E_5^3-2K_4^{28}$.

terminus exposed to the water solvent molecules. Our results therefore support our conjecture that the salt bridge ladder at the junction between the two β -sheet units stabilizes the Osaka mutant whereas such stabilizing salt bridges are missing in the wild type. We note that our results agree with a previous study of HET-s(218–289) fungal prion fibrils that also showed the crucial role that certain salt bridges can play for the stability of aggregates.⁴⁶

Water-Mediated Entropic Forces Favor Fibril Formation for the Osaka Mutant. The NMR fibril models of both the wild-type and the Osaka mutant⁷ aggregates are characterized by a hollow core that can contain structured water forming a hydrogen-bonded network with the exposed side chains.^{19,47} However, the mutant has a cavity that is more than twice as large as that of the wild type, Table 1. This difference likely affects both the toxicity and the rate of aggregation of the two forms.

For the $\text{A}\beta$ wild type, the pore is formed by a pocket made of the A21, D23, K28, A30, I32, and L34 side chains.³⁷ We approximate the pore diameter for the first and second β -sheets by the distance between the C_α -atoms of the D23 and I32 residues of the U-shaped subunits as the distance between these two amino acids approximately corresponds to the diameter of the pore. This distance is averaged over the last 25 ns of the trajectories. For the Osaka mutant, the pore is formed by a pocket of side chains consisting of residues ⁴FRHDSGYEVH¹² and ²⁹AIIGLMVGGVV³⁹ in the adjacent U-shaped subunits. Similarly to the wild type, we define the pore size as the average of the distances distance between the C_α of H6 and M35 residues measured over the last 25 ns of the respective trajectories. Again this distance approximates well the pore diameter. We find no water molecules within the dry two-sheet interface that consists of ³¹GLMVG³⁵ residues (the dry interface results from the hydrophilic nature of this segment of Osaka mutant); however, the snapshots of $\text{A}\beta$ wild type in Figure 7 show water molecules between the two β -sheets.

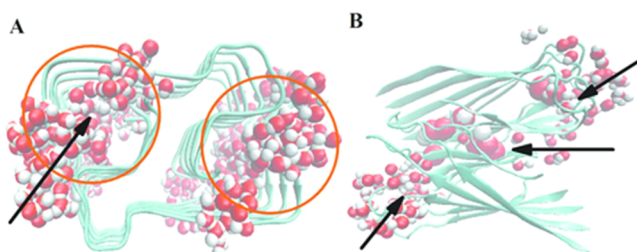


Figure 7. Wild-type $\text{A}\beta$ fibril and Osaka mutant oligomer hydration pores. The distribution of water molecules in Osaka mutant (A) and $\text{A}\beta$ fibril models within the hydrated cavity (B).

The flow of water through the pores was measured using the VMD visualization software. For this purpose, the principle axes of the oligomers are aligned with the xyz axes such that the flow of water is directed along the z axis. The z -coordinates of the center of mass of the outer pore-residues mark the vertical extension of the pore. Water molecules outside of the pore carry a tag 0, after entering from the $+z$ or $-z$ side of the pore this tag is set to +1 or -1. Exiting the pore, the tag is reset to 0; however, a permeation event requires that a water molecule with +1 (-1) tag exits the pore at the end with $-z$ ($+z$) coordinate. Hence, water molecules that enter and exit at the same side of the pore are not counted as permeation events.

The pore size of the wild type $\text{A}\beta$ fibril model averaged over three trajectories is $9.9 \pm 2.1 \text{ \AA}$ for the first β -sheet, and for the second β -sheet it is $11.1 \pm 1.0 \text{ \AA}$ (Table 1). A similar measurement for the Osaka mutant indicates a much wider inner pore diameter: for the first β -sheet the pore diameter is $18.2 \pm 0.2 \text{ \AA}$, and for the second β -sheet it is $20.8 \pm 0.4 \text{ \AA}$ (Table 1). To quantify the effect of the pore size on hydration and water mobility, we have calculated the number (averaged over the entire 100 ns simulation) of water molecules per pore, and the rate of water permeation (measured over the last 40 ns). At start, the channels of both wild type and the Osaka mutant oligomers are empty. Over the course of the simulation, surrounding bulk water moves in and fills these channels, which remain occupied by water molecules during the rest of the 100 ns simulation. The average number of water molecules (calculated as a sum of water molecules in the first and the second β -sheet) inside the Osaka mutant fibril is about 61 water molecules (Table 1) whereas only about 21 water molecules are found in the $\text{A}\beta$ wild type fibril (Table 1).

The cavity in amyloid oligomers results from the water-mediated face-to-face packing of β -sheet pairs hold together by the intermain-chain hydrogen bonding networks that are characteristic for amyloids.⁴⁸ It was found recently by a combination of neutron scattering experiments and molecular dynamic simulations that the fibril form of the tau protein has higher diffusion coefficient and water mobility than that of the monomer.⁴⁹ This increased hydration and water mobility may promote fibril formation through an increase in the entropy of hydration water.^{49,50} This is because the association of monomers involves the release of water molecules whose distribution becomes more disordered. The resulting large gain in entropy is only partially compensated by the ordering of the peptides forming ordered interpeptide hydrogen bonds.⁵¹ In our case, the flow rate of water molecules passing through the pore in the Osaka mutant fibril oligomers is about 30 water molecules per nanosecond whereas the corresponding values for the wild type is about 12 water molecules per nanosecond (Table 1). The more than twice larger flow rate in the Osaka mutant therefore likely leads to entropic effects that encourage fibril formation,⁵⁰ similar to what has been recently shown for tau aggregation.⁴⁹

Note that the twice larger flow rate and the larger number of interior water molecules could also explain the higher toxicity of the Osaka mutant.⁵² One of the proposed mechanisms for neurotoxicity in Alzheimer's disease⁵³ is the formation of an amyloid-pore or channel in the cell membrane by $\text{A}\beta$ -aggregates. Such pores create ion channels that leads to oligomer-mediated toxicity through membrane leakage.⁵³ Hence, the presence of water molecules and their penetration into the oligomer cavity supports the cell membranes leakage mechanism of toxicity of amyloid oligomers, and the observed twice higher flow rate and number of water molecules inside the pores correlates with the Osaka mutant's higher toxicity. The pore sizes are comparable to previous experiments that have shown the potential role of such hydrated channel in toxicity.⁵⁴

CONCLUSION

Multiple explicit-solvent molecular dynamic simulations of the 2-fold aggregates of $\text{A}\beta$ wild type and its single residues deletion mutant E22 (Osaka mutant) were carried out to compare the wild-type with a mutant that *in vivo* is more infective and prone to aggregation. We find that Osaka mutant

fibrils are much more stable than wild-type fibrils, and that this difference originates from the formation of a larger number of intra- and intermolecular salt bridges in the mutant. Spirig et al.⁹ have proposed a prion-like behavior for the Osaka mutant, and $A\beta$ aggregation in general, highlighting the need for an in-depth understanding of the seeding mechanism through which Osaka mutant peptides induce $A\beta$ wild-type aggregation. Our results suggest that the more stable conformation of the Osaka mutant fibril serves as a stable nucleus for the wild-type monomers to take the unique quaternary structure of the mutant, a scenario that is consistent with the recent strain-specific traits hypothesis of Alzheimer diseases. The underlying idea that the wild-type monomers are flexible and assume their structure depending on interaction with environment and other molecules is also in agreement with the existence of various of polymorphic forms observed previously including most interestingly the 3-fold conformation recently reported Nussinov and co-workers.⁵⁵

In addition to its higher stability, the Osaka mutant fibril also has a wider hydration channel that may play a significant role for its toxicity and aggregation. The wider hollow channel in the Osaka mutant is hydrated as in the wild type but the rate of flow of water is more than 2-fold for the mutant. The larger hydration rate and expulsion of the water molecules could promote formation of fibers by increasing hydration water entropy when compared to the similar-sized oligomer. The observed difference in water penetrating of the mutant and wild type can explain the experimentally observed differences in toxicity if one assumes pore formation and membrane leakage as toxicity mechanism.

■ AUTHOR INFORMATION

Corresponding Author

*E-mail: uhansmann@ou.edu.

Notes

The authors declare no competing financial interest.

■ ACKNOWLEDGMENTS

We thank Dr. Claudio Luchinat for providing the atomic coordinates of the $A\beta$ 40 fibril models. This work used resources of the National Energy Research Scientific Computing Center, which is supported by the Office of Science of the U.S. Department of Energy under contract no. DE-AC02-05CH11231. Other parts of the simulations were done on the BOOMER cluster of the University of Oklahoma. We acknowledge financial support from NSF CHE-1266256 and OCAST HR14-129.

■ REFERENCES

- Eisenberg, D.; Jucker, M. The Amyloid State of Proteins in Human Diseases. *Cell* **2012**, *148*, 1188–1203.
- Nasica-Labouze, J.; Nguyen, P. H.; Sterpone, F.; Berthoumieu, O.; Buchete, N. V.; Coté, S.; De Simone, A.; Doig, A. J.; Faller, P.; Garcia, A.; et al. Amyloid Beta Protein and Alzheimer's Disease: When Computer Simulations Complement Experimental Studies. *Chem. Rev.* **2015**, *115*, 3518–3563.
- Blennow, K.; de Leon, M. J.; Zetterberg, H. Alzheimer's Disease. *Lancet* **2006**, *368*, 387–403.
- Shankar, G. M.; Li, S. M.; Mehta, T. H.; Garcia-Munoz, A.; Shepardson, N. E.; Smith, I.; Brett, F. M.; Farrell, M. A.; Rowan, M. J.; Lemere, C. A.; et al. Amyloid-Beta Protein Dimers Isolated Directly from Alzheimer's Brains Impair Synaptic Plasticity and Memory. *Nat. Med.* **2008**, *14*, 837–842.
- Tycko, R. Amyloid Polymorphism: Structural Basis and Neurobiological Relevance. *Neuron* **2015**, *86*, 632–645.
- Qiang, W.; Yau, W. M.; Luo, Y. Q.; Mattson, M. P.; Tycko, R. Antiparallel Beta-Sheet Architecture in Iowa-Mutant Beta-Amyloid Fibrils. *Proc. Natl. Acad. Sci. U. S. A.* **2012**, *109*, 4443–4448.
- Schutz, A. K.; Vagt, T.; Huber, M.; Ovchinnikova, O. Y.; Cadalbert, R.; Wall, J.; Guntert, P.; Bockmann, A.; Glockshuber, R.; Meier, B. H. Atomic-Resolution Three-Dimensional Structure of Amyloid Beta Fibrils Bearing the Osaka Mutation. *Angew. Chem., Int. Ed.* **2015**, *54*, 331–335.
- Lu, J. X.; Qiang, W.; Yau, W. M.; Schwieters, C. D.; Meredith, S. C.; Tycko, R. Molecular Structure of Beta-Amyloid Fibrils in Alzheimer's Disease Brain Tissue. *Cell* **2013**, *154*, 1257–1268.
- Spirig, T.; Ovchinnikova, O.; Vagt, T.; Glockshuber, R. Direct Evidence for Self-Propagation Different Amyloid-Beta Fibril Conformations. *Neurodegener. Dis.* **2014**, *14*, 151–159.
- Stohr, J.; Watts, J. C.; Mensinger, Z. L.; Oehler, A.; Grillo, S. K.; DeArmond, S. J.; Prusiner, S. B.; Giles, K. Purified and Synthetic Alzheimer's Amyloid Beta ($A\beta$) Prions. *Proc. Natl. Acad. Sci. U. S. A.* **2012**, *109*, 11025–11030.
- Tomiyama, T.; Matsuyama, S.; Iso, H.; Umeda, T.; Takuma, H.; Ohnishi, K.; Ishibashi, K.; Teraoka, R.; Sakama, N.; Yamashita, T.; et al. A Mouse Model of Amyloid Beta Oligomers: Their Contribution to Synaptic Alteration, Abnormal Tau Phosphorylation, Glial Activation, and Neuronal Loss in Vivo. *J. Neurosci.* **2010**, *30*, 4845–4856.
- Cloe, A. L.; Orgel, J.; Sachleben, J. R.; Tycko, R.; Meredith, S. C. The Japanese Mutant $A\beta$ (Δ E22- $A\beta$ (1–39)) Forms Fibrils Instantaneously, with Low-Thioflavin T Fluorescence: Seeding of Wild-Type $A\beta$ (1–40) into Atypical Fibrils by Δ E22- $A\beta$ (1–39). *Biochemistry* **2011**, *50*, 2026–2039.
- Takeda, T.; Klimov, D. K. Replica Exchange Simulations of the Thermodynamics of Abeta Fibril Growth. *Biophys. J.* **2009**, *96*, 442–52.
- Blinov, N.; Dorosh, L.; Wishart, D.; Kovalenko, A. Association Thermodynamics and Conformational Stability of Beta-Sheet Amyloid Beta(17–42) Oligomers: Effects of E22Q (Dutch) Mutation and Charge Neutralization. *Biophys. J.* **2010**, *98*, 282–296.
- Berhanu, W. M.; Hansmann, U. H. E. In *Biomolecular Modelling and Simulations*; KarabenchevaChristova, T., Ed.; Elsevier Academic Press Inc.: San Diego, 2014; Vol. 96, pp 113–141.
- Ma, B. Y.; Nussinov, R. Simulations as Analytical Tools to Understand Protein Aggregation and Predict Amyloid Conformation. *Curr. Opin. Chem. Biol.* **2006**, *10*, 445–452.
- Han, W.; Schulten, K. Fibril Elongation by $A\beta$ (17–42): Kinetic Network Analysis of Hybrid-Resolution Molecular Dynamics Simulations. *J. Am. Chem. Soc.* **2014**, *136*, 12450–12460.
- Cheon, M.; Hall, C. K.; Chang, I. Structural Conversion of $A\beta$ 17–42 Peptides from Disordered Oligomers to U-Shape Protofilaments Via Multiple Kinetic Pathways. *PLoS Comput. Biol.* **2015**, *11*, e1004258.
- Alred, E. J.; Phillips, M.; Berhanu, W. M.; Hansmann, U. H. E. On the Lack of Polymorphism in $A\beta$ -Peptide Aggregates Derived from Patient Brains. *Protein Sci.* **2015**, *24*, 923–935.
- Bertini, I.; Gonnelli, L.; Luchinat, C.; Mao, J. F.; Nesi, A. A New Structural Model of A Beta(40) Fibrils. *J. Am. Chem. Soc.* **2011**, *133*, 16013–16022.
- GhattyVenkataKrishna, P. K.; Uberbacher, E. C.; Cheng, X. L. Effect of the Amyloid Beta Hairpin's Structure on the Handedness of Helices Formed by Its Aggregates. *FEBS Lett.* **2013**, *587*, 2649–2655.
- Hornak, V.; Abel, R.; Okur, A.; Strockbine, B.; Roitberg, A.; Simmerling, C. Comparison of Multiple Amber Force Fields and Development of Improved Protein Backbone Parameters. *Proteins: Struct., Funct., Genet.* **2006**, *65*, 712–725.
- Jorgensen, W. L.; Chandrasekhar, J.; Madura, J. D.; Impey, R. W.; Klein, M. L. Comparison of Simple Potential Functions for Simulating Liquid Water. *J. Chem. Phys.* **1983**, *79*, 926–935.
- Pronk, S.; Pall, S.; Schulz, R.; Larsson, P.; Bjelkmar, P.; Apostolov, R.; Shirts, M. R.; Smith, J. C.; Kasson, P. M.; van der Spoel,

- D.; et al. Gromacs 4.5: A High-Throughput and Highly Parallel Open Source Molecular Simulation Toolkit. *Bioinformatics* **2013**, *29*, 845–854.
- (25) Hess, B. P-Lincs: A Parallel Linear Constraint Solver for Molecular Simulation. *J. Chem. Theory Comput.* **2008**, *4*, 116–122.
- (26) Miyamoto, S.; Kollman, P. A. Settle - an Analytical Version of the Shake and Rattle Algorithm for Rigid Water Models. *J. Comput. Chem.* **1992**, *13*, 952–962.
- (27) Bussi, G.; Donadio, D.; Parrinello, M. Canonical Sampling through Velocity Rescaling. *J. Chem. Phys.* **2007**, *126*, 014101.
- (28) Bussi, G.; Zykova-Timan, T.; Parrinello, M. Isothermal-Isobaric Molecular Dynamics Using Stochastic Velocity Rescaling. *J. Chem. Phys.* **2009**, *130*, 074101.
- (29) Parrinello, M.; Rahman, A. Polymorphic Transitions in Single-Crystals - a New Molecular-Dynamics Method. *J. Appl. Phys.* **1981**, *52*, 7182–7190.
- (30) Humphrey, W.; Dalke, A.; Schulten, K. Vmd: Visual Molecular Dynamics. *J. Mol. Graphics* **1996**, *14*, 33–38.
- (31) Case, D. A.; Cheatham, T. E.; Darden, T.; Gohlke, H.; Luo, R.; Merz, K. M.; Onufriev, A.; Simmerling, C.; Wang, B.; Woods, R. J. The Amber Biomolecular Simulation Programs. *J. Comput. Chem.* **2005**, *26*, 1668–1688.
- (32) Auer, S. Nucleation of Polymorphic Amyloid Fibrils. *Biophys. J.* **2015**, *108*, 1176–1186.
- (33) Genheden, S.; Ryde, U. Will Molecular Dynamics Simulations of Proteins Ever Reach Equilibrium? *Phys. Chem. Chem. Phys.* **2012**, *14*, 8662–8677.
- (34) Genheden, S.; Ryde, U. The Mm/Pbsa and Mm/Gbsa Methods to Estimate Ligand-Binding Affinities. *Expert Opin. Drug Discovery* **2015**, *10*, 449–461.
- (35) Park, J.; Kahng, B.; Hwang, W. Thermodynamic Selection of Steric Zipper Patterns in the Amyloid Cross-Beta Spine. *PLoS Comput. Biol.* **2009**, *5*, e1000492.
- (36) Homeyer, N.; Gohlke, H. Free Energy Calculations by the Molecular Mechanics Poisson-Boltzmann Surface Area Method. *Mol. Inf.* **2012**, *31*, 114–122.
- (37) Zheng, J.; Jang, H.; Ma, B.; Tsai, C. J.; Nussinov, R. Modeling the Alzheimer a Beta(17–42) Fibril Architecture: Tight Intermolecular Sheet-Sheet Association and Intramolecular Hydrated Cavities. *Biophys. J.* **2007**, *93*, 3046–3057.
- (38) Kahler, A.; Sticht, H.; Horn, A. H. Conformational Stability of Fibrillar Amyloid-Beta Oligomers Via Protofilament Pair Formation - a Systematic Computational Study. *PLoS One* **2013**, *8*, e70521.
- (39) Petkova, A. T.; Yau, W. M.; Tycko, R. Experimental Constraints on Quaternary Structure in Alzheimer's Beta-Amyloid Fibrils. *Biochemistry* **2006**, *45*, 498–512.
- (40) Shammas, S. L.; Knowles, T. P. J.; Baldwin, A. J.; MacPhee, C. E.; Welland, M. E.; Dobson, C. M.; Devlin, G. L. Perturbation of the Stability of Amyloid Fibrils through Alteration of Electrostatic Interactions. *Biophys. J.* **2011**, *100*, 2783–2791.
- (41) Fitzpatrick, A. W. P.; Vanacore, G. M.; Zewail, A. H. Nanomechanics and Intermolecular Forces of Amyloid Revealed by Four-Dimensional Electron Microscopy. *Proc. Natl. Acad. Sci. U. S. A.* **2015**, *112*, 3380–3385.
- (42) Kabsch, W.; Sander, C. Dictionary of Protein Secondary Structure - Pattern-Recognition of Hydrogen-Bonded and Geometrical Features. *Biopolymers* **1983**, *22*, 2577–2637.
- (43) Schledorn, M.; Meier, B. H.; Böckmann, A. Alternative Salt Bridge Formation in $\text{A}\beta$ - a Hallmark of Early-Onset Alzheimer's Disease? *Front. Mol. Biosci.* **2015**, *2*, 2.
- (44) Meier, B. H.; Böckmann, A. The Structure of Fibrils from 'Misfolded' Proteins. *Curr. Opin. Struct. Biol.* **2015**, *30*, 43–49.
- (45) Berhanu, W. M.; Hansmann, U. H. E. Structure and Dynamics of Amyloid-Beta Segmental Polymorphisms. *PLoS One* **2012**, *7*, e41479.
- (46) Lange, A.; Gattin, Z.; Van Melckebeke, H.; Wasmer, C.; Soragni, A.; van Gunsteren, W. F.; Meier, B. H. A Combined Solid-State Nmr and Md Characterization of the Stability and Dynamics of the Het-
- S(218–289) Prion in Its Amyloid Conformation. *ChemBioChem* **2009**, *10*, 1657–1665.
- (47) Fitzpatrick, A. W. P.; Debelouchina, G. T.; Bayro, M. J.; Clare, D. K.; Caporini, M. A.; Bajaj, V. S.; Jaroniec, C. P.; Wang, L. C.; Ladizhansky, V.; Muller, S. A.; et al. Atomic Structure and Hierarchical Assembly of a Cross-Beta Amyloid Fibril. *Proc. Natl. Acad. Sci. U. S. A.* **2013**, *110*, 5468–5473.
- (48) Chen, S. W.; Drakulic, S.; Deas, E.; Ouberai, M.; Aprile, F. A.; Arranz, R.; Ness, S.; Roodveldt, C.; Guilliams, T.; De-Genst, E. J.; et al. Structural Characterization of Toxic Oligomers That Are Kinetically Trapped During Alpha-Synuclein Fibril Formation. *Proc. Natl. Acad. Sci. U. S. A.* **2015**, *112*, E1994–E2003.
- (49) Fichou, Y.; Schiro, G.; Gallat, F. X.; Laguri, C.; Moulin, M.; Combete, J.; Zamponi, M.; Hartlein, M.; Picart, C.; Mossou, E.; et al. Hydration Water Mobility Is Enhanced around Tau Amyloid Fibers. *Proc. Natl. Acad. Sci. U. S. A.* **2015**, *112*, 6365–6370.
- (50) Sun, T. J.; Lin, F. H.; Campbell, R. L.; Allingham, J. S.; Davies, P. L. An Antifreeze Protein Folds with an Interior Network of More Than 400 Semi-Clathrate Waters. *Science* **2014**, *343*, 795–798.
- (51) Thirumalai, D.; Reddy, G.; Straub, J. E. Role of Water in Protein Aggregation and Amyloid Polymorphism. *Acc. Chem. Res.* **2012**, *45*, 83–92.
- (52) Ovchinnikova, O. Y.; Finder, V. H.; Vodopivec, I.; Nitsch, R. M.; Glockshuber, R. The Osaka Fad Mutation E22 Δ Leads to the Formation of a Previously Unknown Type of Amyloid- β Fibrils and Modulates $\text{A}\beta$ Neurotoxicity. *J. Mol. Biol.* **2011**, *408*, 780–791.
- (53) Quist, A.; Doudevski, L.; Lin, H.; Azimova, R.; Ng, D.; Frangione, B.; Kagan, B.; Ghiso, J.; Lal, R. Amyloid Ion Channels: A Common Structural Link for Protein-Misfolding Disease. *Proc. Natl. Acad. Sci. U. S. A.* **2005**, *102*, 10427–10432.
- (54) Lashuel, H. A.; Hartley, D.; Petre, B. M.; Walz, T.; Lansbury, P. T. Neurodegenerative Disease - Amyloid Pores from Pathogenic Mutations. *Nature* **2002**, *418*, 291–291.
- (55) Xiao, Y. L.; Ma, B. Y.; McElheny, D.; Parthasarathy, S.; Long, F.; Hoshi, M.; Nussinov, R.; Ishii, Y. $\text{A}\beta(1–42)$ Fibril Structure Illuminates Self-Recognition and Replication of Amyloid in Alzheimer's Disease. *Nat. Struct. Mol. Biol.* **2015**, *22*, 499–505.